


Article

Damage Assessment and Progressive Collapse Resistance of a Long-Span Prestressed Double-Layer Composite Torsional Reticulated Shell

Xiaohui Zhang ¹ , Haifang Long ², Jiyang Zhang ³, Bo Shen ³ and Yonghui Hou ^{1,*}

¹ Key Laboratory of C & PC Structures of Ministry of Education, National Prestress Engineering Research Center, Southeast University, Nanjing 211189, China; zhangxiaohui@seu.edu.cn

² The College of Humanities and Science, Guizhou Minzu University, Guiyang 550025, China; 16b933059@stu.hit.edu.cn

³ Space Structures Research Center, GuiZhou University, Guiyang 550003, China; zjy_str@163.com (J.Z.); bshen@gzu.edu.cn (B.S.)

* Correspondence: 230179421@seu.edu.cn

Received: 31 July 2020; Accepted: 27 August 2020; Published: 30 August 2020



Abstract: Long-span prestressed double-layer composite torsional reticulated shells have beautiful shapes, which make them a solution widely applied in public buildings requiring long-span structures, such as airports and stadiums. However, once the progressive collapse occurs, this will cause serious issues. There are few studies on the damage assessment of long-span spatial structures under accidental loads. This paper proposes a new dynamic damage evaluation index that takes into account the displacement and the cumulative plastic energy dissipation to evaluate the damage of the long-span prestressed double-layer composite torsional reticulated shell. Sleeve structures were applied to the long-span space structures to study their control effect on structural damage. The equivalent load transient unloading method was used to analyze the dynamic time history of the structure. Results show that the structure suffered severe damage and progressive collapse failure after removing four nodes at different positions near the supports. In the position where the plastic hinges first appear and the position with the maximum displacement, the sleeve structures have a poor damage control effect on the structure. Arranging the two sleeve structures in the position of maximum stress, the damage of the structure can be controlled, thus reducing the severe damage and progressive collapse failure to basic intact damage.

Keywords: symmetrical long-span spatial structure; dynamic damage index; progressive collapse; sleeve structure; damage level

1. Introduction

Long-span spatial structures offer structurally efficient solutions in aesthetically appealing shapes, and many of them have a kind of symmetrical beauty. Currently, they are widely applied for design solutions that cover large pedestrian flows, such as gymnasiums and airports. Because often designed to cover public spaces with a high user density, the understanding of their behavior under accidental loads is of paramount importance. Although long-span space structures are designed to have high redundancy, the occurrence of an accident of progressive collapse under the action of accidental loads such as impacts, explosions, snow loads, and terrorist attacks may cause immeasurable consequences. The collapse of long-span spatial structures is not uncommon. For example, the roof of the Hartford Civic Center Gymnasium collapsed under snow load [1]. In the design of the Siemens Arena in Denmark, the material of the support components were overestimated by 50%, leading to the progressive collapse of the structure due to insufficient strength [2]. Due to a long-term exposure to

the outdoor environment, the glued part of the joint of the BadReichenhall in Germany experienced damages until failure, resulting in the progressive collapse of the structure [3]. Additionally, the roof of the Moscow Basmani market collapsed due to adverse environmental conditions caused by a snow load, killing 66 people in a dramatic accident [4]. Although the understanding of the progressive collapse failure of long-span spatial structures is of primary importance to ensure the safety of a wide range of public spaces, current research mainly focuses on the progressive collapse of frame structures [5–8], and on their corresponding codes [9–12].

As long-span spatial structures become more and more used widely, it is necessary to conduct in-depth investigations into their progressive collapse. Relevant scholars investigated the criterion of failure of long-span spatial structure collapse. Xu et al. [13] carried out numerical simulation and experiment on the Kiewitt Lamella and on geodesic single-layer latticed domes. Based on the maximum displacement response of the structure, the criterion of the progressive collapse was established, and the collapse behavior of the structure studied. Zhu et al. [14] applied the theory of structural vulnerability to a single-layer reticulated shell. They used displacement as an evaluation index for the performance of the structure and further studied its progressive collapse. Sheidaii and Parke [15] proposed a method based on an energy calculation to determine the dynamic jump instability of space truss structures, and successfully applied it to the jump instability analysis of double-layer space truss structures. Zhou et al. [16] proposed a failure criterion based on the damage accumulation theory to study the progressive collapse of a long-span spatial structure, which was verified by full-scale test. Despite the performed research, there is still no consistent criterion for judging the progressive collapse failure of long-span spatial structures. From the above analysis, it can be seen that the displacement and the plastic energy dissipation are two important indexes in the study of the progressive collapse of long-span spatial structures. However, these two indexes are considered separately in the study of the progressive collapse of structures, an aspect that may lead to a certain level of inaccuracy. When only considering the maximum displacement index of the structure, the specific failure position of the structure can be assessed, but not taking into consideration the overall plastic damage accumulation degree under the load. Differently, when only considering the plastic energy dissipation, the specific failure location of the structure cannot be assessed, because one energy measure may correspond to multiple failure possibilities. In order to tackle this problem, this paper considers both displacement and energy dissipation, and proposes a combination of the maximum displacement and plastic energy dissipation index to assess damages of long-span spatial structures.

As the progressive collapse of long-span space structures may occur under the action of different unexpected loads, several methods to avoid it have been developed by different scholars. The transverse connection beam method and the ring reinforced truss method, proposed by Li [17] can effectively improve the progressive collapse resistance of the long-span structure. Zhu et al. [18] found that the structural integrity of the system increases with the increase in the bending stiffness of the longitudinal connection truss, which allowed for the improvement of the progressive collapse resistance of the structure. Despite the fact that the described methods were shown to be successfully applicable for the improvement of the progressive collapse resistance of long-span space structures, they often negatively altered the aesthetic of the structures. Moreover, these design methods can not completely solve the structural failure caused by the instability of the main compression members, which determine a poor ductility. The sleeve structure is an instability control component with excellent ductility and hysteretic properties. Compared with the traditional round steel pipe, the compressive bearing capacity of the sleeve structure is significantly improved [19]. Hu et al. [20] and Shen et al. [21] conducted experiments on sleeve structures. The results showed that the sleeve structures have good static performance and hysteretic behaviors. Zhang et al. [22] applied the simplified theory to analyze the sleeve structure and pointed out the factors affecting the contact between the core and the sleeve, and parametric studies were performed to investigate the effects of the factors on the improvement of the ultimate bearing capacities of the sleeve structures. A parametric study was conducted to quantify how essential factors, including the core protrusion length above the sleeve–stiffness ratio of the core-to-sleeve

core–slenderness ratio and gap between the core and sleeve affect the mechanical behaviors of the sleeve structures [23]. At present, the research of sleeve structures is mainly on the component level, and the application of long-span spatial structures has not been studied. In this paper, the control effect of sleeve structures on the failure of long-span spatial structures will be studied in depth.

At present, there are two kinds of analysis methods for long-span spatial reticulated shells. One is the quasi shell method of continuous analysis. Based on the shell theory, Sadamoto et al. [24,25] use the meshfree method to analyze the buckling of stiffened shells and shells with and without cutouts, which provides a theoretical study for the buckling analysis of continuous shells. Due to the quasi shell method, continuous analysis needs to have equal and back substitution processes as its calculation accuracy is not as good as that of the discrete finite element method. At the same time, this method needs to solve the analytical solution, which can not be used for complex and irregular structures. The other is the finite element method of discretization analysis. This method adopts the matrix expression equation suitable for computer operation to analyze the grid structure. The whole structure stiffness matrix and equation are established by the stiffness matrix set of each basic element, and then the boundary conditions are introduced to solve the equation. The finite element method of discretization analysis has become the main method of spatial grid structure analysis. In this paper, the discrete finite element method was adopted.

In the research of the progressive collapse of long-span spatial structures, most scholars study the structural failure caused by the failure of a single key member, while in this paper, the structural failure caused by key node failure is studied. The maximum displacement and cumulative plastic energy dissipation were introduced to evaluate the damage degrees of long-span spatial structures, which are more convenient and reasonable. Moreover, this paper adopts a new method to resist progressive collapse by placing sleeve structures in the long-span spatial structure.

This paper investigates a long-span prestressed double-layer composite torsional reticulated shell (LSPDLCTRS) with a symmetrical aesthetic shape. Firstly, based on the proposed dynamic damage evaluation index of the combination of displacement and plastic energy dissipation, the damage of the structure is evaluated after the key nodes are removed. Then, sleeve structures are arranged for the structures with severe damage and progressive collapse, respectively. The control effect of sleeve structure arrangement on damage is studied and, finally, the principles of sleeve structure arrangement in long-span spatial structures are given.

2. A Composite Index of Displacement and Plastic Energy Dissipation

A calculation example is performed considering the two indexes of displacement and plastic energy dissipation, respectively. A plane truss consisting of round steel pipes with a size of 60 mm × 3.0 mm was selected, with each node of the upper chord exerting a concentrated load of 70 kN. The dotted line indicates the pipes A, B, and C that have to be removed, as shown in Figure 1a.

Under the action of loads, the maximum displacement of the structure is 3113 mm when the member A is removed, as shown in Figure 1b, while the plastic energy dissipation of the structure is 0. If only considering the displacement index, according to the relevant criteria the structure should be collapsed, but it can be seen that the main body of it has almost not been damaged. As only small damages occur locally in the structure, it can be deduced that considering only the displacement index will lead to an inaccurate evaluation of the progressive collapse of the structure.

Because of the symmetric properties of the system, when the member B or the member C are removed, the plastic energy dissipation of the structure is 1.9×10^4 J. Considering only the plastic energy dissipation, it is not possible to determine whether the failure position of the structure is in the member B or C. However, considering that the maximum displacement of the structure is 171 mm, as shown in Figure 1c, which is close to member B, it can be deduced that the failure of the structure occurs in member B. Therefore, the combination of the maximum displacement and plastic energy dissipation can make a more reasonable assessment of the damage degree and the specific failure location of the structure.

The damage degree of the structure is expressed as a combination of the maximum displacement and plastic energy dissipation [26]. A new evaluation index of the damage degree of long-span spatial structures was proposed, which is expressed by the dynamic damage index D .

$$D = \frac{\delta_m}{\delta_u} + \frac{\int dE}{Q_y \delta_u}, \quad (1)$$

where D is the dynamic damage index, which measures the damage degree of the structure; δ_m represents the maximum displacement of the structure in the process of failure; δ_u represents the maximum displacement of the intact structure under static load; Q_y represents the total bearing reaction of the intact structure under static load; $\int dE$ represents the cumulative plastic energy dissipation of the structure in the process of failure. The first term of Formula (1) is the ratio of the maximum displacement response of the structure in the failure process to the ultimate displacement of the intact structure under static load, which reflects the specific failure position of the structure; the second term is the ratio of the cumulative plastic energy dissipation of the residual structure to the ultimate energy consumption of the intact structure in the failure process, reflecting the development of the plastic energy dissipation of the structure.

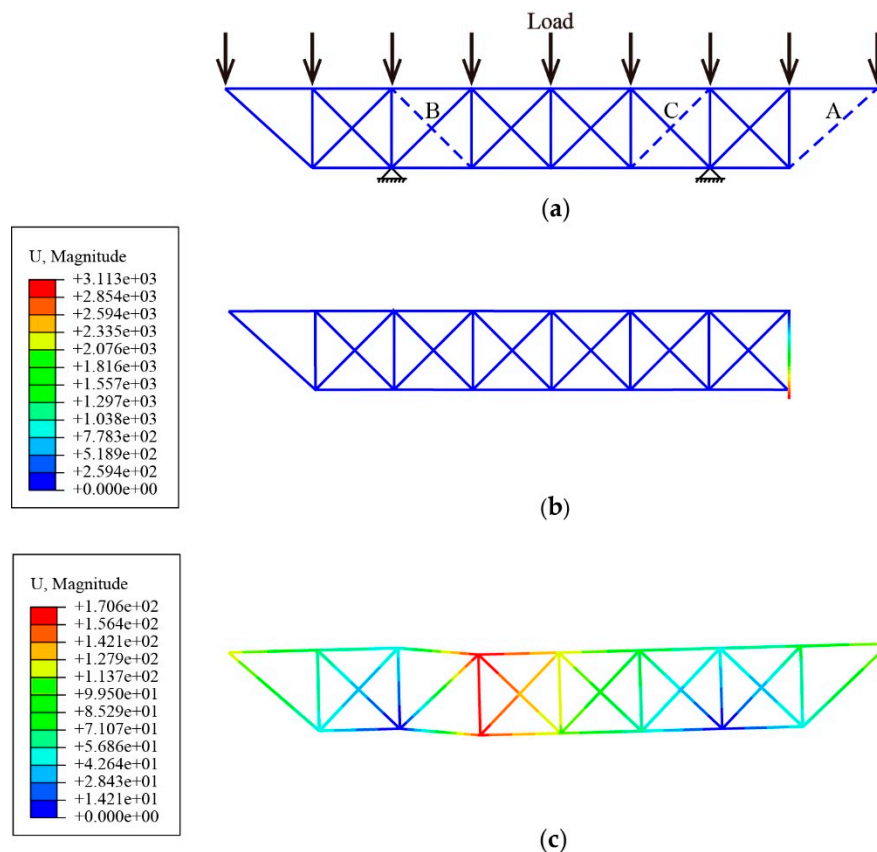


Figure 1. Calculation example: (a) Intact structural plane truss; (b) Displacement diagram after the removal of the A member; (c) Displacement diagram after the removal of the B member.

3. Structural Failure Analysis

3.1. Structural Model

The case study of this paper is the gymnasium of Qingyuan City in the Guangdong Province, China, which is beautiful in shape and full of symmetrical beauty, as shown in Figure 2. It can be seen from Figures 3 and 4 that the upper part of the structure is composed of six torsional reticulated

shells, which are connected with the hexagonal three-dimensional flat grid and the daylighting areas. The torsional reticulated shell is saddle shaped with negative Gaussian curvature, which can increase the stiffness while obtaining beautiful shape. The lower part of the structure is composed of six reinforced concrete columns. Different from the single-layer reticulated shell, the structure studied in this paper is a double-layer reticulated shell structure, in which all the connecting nodes of the members are hinged, as shown in Figure 5. The area of the building is 5450 m². The diagonal span of the structure is 68,418 m, the cantilever is 12,615 m, and the structure height is 2.8 m.



Figure 2. The Gymnasium.

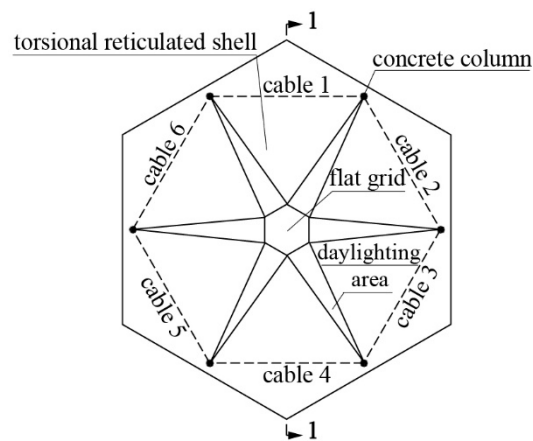


Figure 3. The plan of the structure.

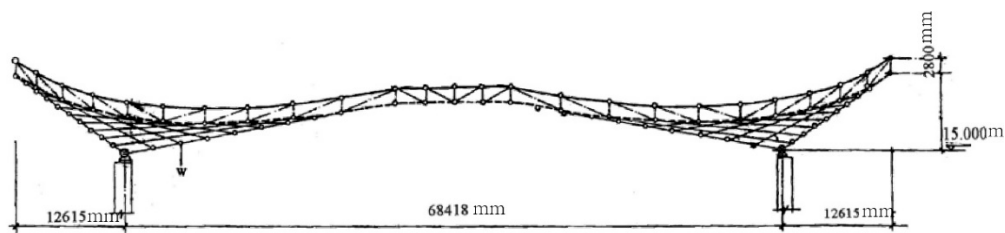


Figure 4. Section of the structure 1–1.

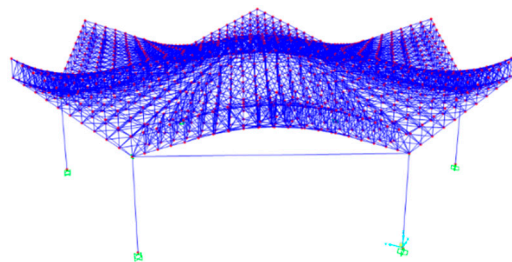


Figure 5. Structural 3D model.

The structural members are selected from the following sections: solid round steel rods with an equivalent size of φ 80 mm of prestressed cable, with a standard value of tensile strength of 1870 MPa; the dimensions of the roof steel pipes are: φ 60 mm \times 3.5 mm, φ 68 mm \times 3.5 mm, φ 76 mm \times 3.5 mm, φ 83 mm \times 3.5 mm, φ 89 mm \times 3.5 mm, φ 95 mm \times 3.5 mm, φ 102 mm \times 3.5 mm, φ 114 mm \times 4 mm, φ 121 mm \times 4 mm, φ 133 mm \times 4 mm, φ 140 mm \times 4.5 mm, φ 152 mm \times 4.5 mm, φ 168 mm \times 4.5 mm, φ 180 mm \times 5 mm, φ 194 mm \times 5 mm, φ 203 mm \times 6 mm, φ 219 mm \times 6 mm, φ 219 mm \times 8 mm, φ 245 mm \times 6.5 mm, φ 273 mm \times 6.5 mm, φ 299 mm \times 7.5 mm, φ 351 mm \times 8.0 mm, the steel is Q345; the cross-sectional size of the concrete column is 1200 mm \times 1200 mm. SAP2000 is used to establish the model, and the version of software used in this paper is SAP2000 17.3. Rubber bearings are adopted at the connection of the upper roof and lower columns. The plane size of the rubber bearing is 500 mm \times 750 mm, with a total thickness of 67 mm. The rubber bearing is simulated as a spring element with an effective stiffness of 7780 kN/m, and an infinite vertical stiffness.

3.2. Sensitive Areas Analysis of the Structure

We define as sensitive areas the weak parts of the structure, with the key members or nodes of the structure that are located in those areas. The sensitive areas are determined by the regions with a larger eigenvalue buckling response. The eigenvalue buckling analysis of the structure was carried out, and the first four modes were selected, as shown in Figure 6. F. Fu et al. [27] studied the progressive collapse performance of a double-layer space truss structure and concluded that the members at the supports are most critical. Hence, we considered the vicinity of the supports also as sensitive areas. Because of its symmetric structure, according to the first four eigenvalue buckling modes and support areas, the sensitive areas of the structure can be represented by one quarter of it, as shown in Figure 7.

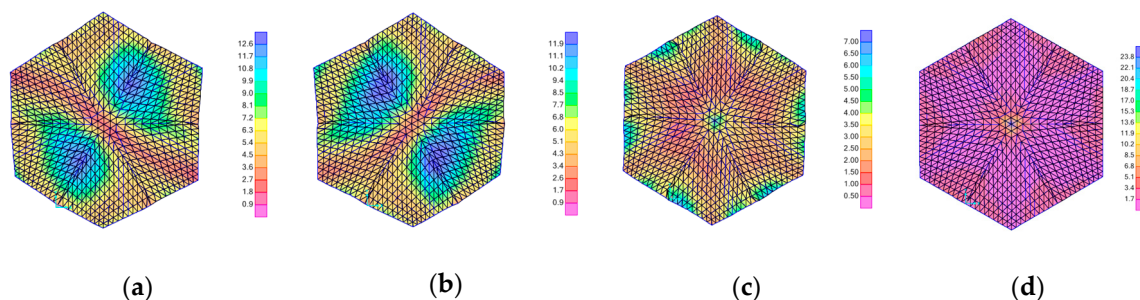


Figure 6. Eigenvalue buckling modes: (a) First-order mode; (b) Second-order mode; (c) Third-order mode; (d) Fourth-order mode.

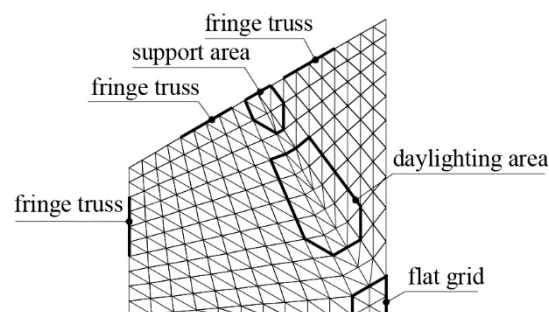


Figure 7. Sensitive areas (one quarter of structure).

It can be seen from Figure 7 that the sensitive areas are located in the support area, in the daylighting area, in the flat grid area, and in the fringe truss. Because the high redundancy of the long-span prestressed the double-layer composite torsion lattice shell, the removal of a single key member has a minor impact on it. To fully understand the failure mechanism of the structure,

its damages after removing the nodes were investigated with the removed nodes that were located in the defined sensitive areas.

3.3. Simulation of Failure Nodes

When studying the progressive collapse of structures, it is necessary to consider their dynamic response. In particular, the dynamic load comes from the structural vibration caused by the sudden failure of members or nodes. In this paper, the equivalent load transient unloading method was used to analyze the progressive collapse dynamic time history of the LSPDLCTRS.

The main analysis steps of the equivalent load transient unloading method are shown in Figure 8. Assuming the sudden failure of the node N under the action of unexpected loads, the members connected to the node were removed. Firstly, the inner forces P_1 , P_2 and P_3 of the middle three members under the static load q were solved, and then the inner forces were reacted on the structure. Secondly, the failure process of the three members was transformed into the unloading process of loads P_1 , P_2 and P_3 with time, thus defining the time history analysis curve shown in Figure 9. In Figure 9, t_1 represents the failure time of the removed member, which is generally no greater than $0.1T$. T is the basic period of the remaining structure. t_2 represents the time of structural vibration stabilization. Finally, in the dynamic time history analysis, the load q was applied in the structure, and the loads P_1 , P_2 and P_3 were applied, according to Figure 9, while the residual of the structure was forced to vibrate under the loads.

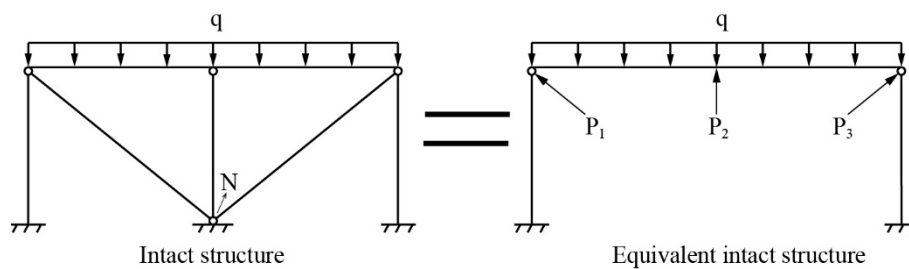


Figure 8. Simulation of the failure node N.

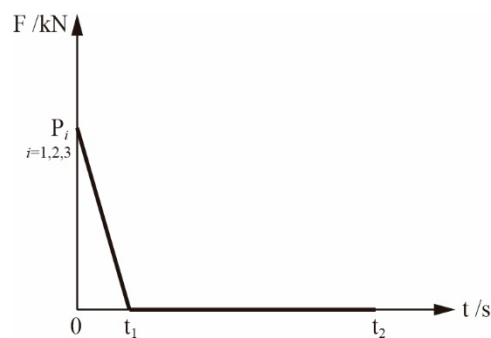


Figure 9. Equivalent load time history curve.

The simulation method of node failure was introduced, which can be applied to the study of progressive collapse of the LSPDLCTRS. The load combination of $1.0DL + 0.25LL$ was adopted in the progressive collapse analysis. DL is the dead load and LL is the live load. The dead load (DL) includes the surface load, the bridle path of the lower chord, and the suspension load of the lower chord, which are 1 kN/m^2 , 0.35 kN/m^2 and 0.5 kN/m^2 , respectively. The live load (LL) is 0.5 kN/m^2 . In this paper, t_1 is 0.1 s and t_2 is 25 s .

3.4. The Criterion of Structural Failure

Based on multiple responses and deformation energy, Nie et al. [28] quantified the different damage states of long-span spatial structures under earthquake action. Zhang [29] et al. used exponential strain energy density and maximum nodal displacement to classify the damage levels of long-span spatial structures. They divided the damage of long-span spatial structures into five damage levels: basic intact, slight damage, medium damage, severe damage, and collapse [28,29]. In this paper, we also divided the structural failure into five damage levels. Based on the dynamic damage index D of Formula (1), $D = 0.2$, $D = 0.4$, $D = 0.7$, and $D = 1.0$ were selected as the boundary values of basic intact, slight damage, medium damage, severe damage, and progressive collapse. The corresponding damage levels were I, II, III, IV, V. When $0 \leq D < 0.2$, the components of the structure were almost in the elastic stage with a small displacement, which did not cause damages to structural elements and equipments, and no repair would be needed after a disaster. When $0.2 \leq D < 0.4$, a small number of components of the structure entered into a plastic stage, still not causing permanent damages and having a not prohibitive repair cost. When $0.4 \leq D < 0.7$, a certain number of components entered into their plastic stage, with the structure experiencing a certain degree of damage. The large displacement encountered by the structure caused a certain degree of damage to the water and electric systems, and to other equipment with a high repair cost after the disaster. When $0.7 \leq D < 1.0$, more components encountered plastic deformations, thus causing serious damage. The displacement of the structure was very large; the water and electric systems, and other equipments would be seriously damaged, and the repair cost would be very high. When $1.0 \leq D$, the structure completely lost its bearing capacity and finally collapsed.

3.5. Intact Structure Analysis

The arc length method was used to analyze the intact LSPDLCTRS, and the static maximum displacement and the ultimate total reaction force of supports of the structure were obtained, as shown in Figure 10. The initial displacement of the structure was positive because the structure moved upward after the prestress was applied, as shown at point O. After the load of $1.0DL + 0.25LL$ was applied to the structure, the displacement started to increase in the opposite direction and became a negative value. Point P represents the ultimate value of the reaction force Q_y of the structural supports, and the value is 32,259 kN. The maximum displacement of the structure is at point Q, and the value is -1424 mm.

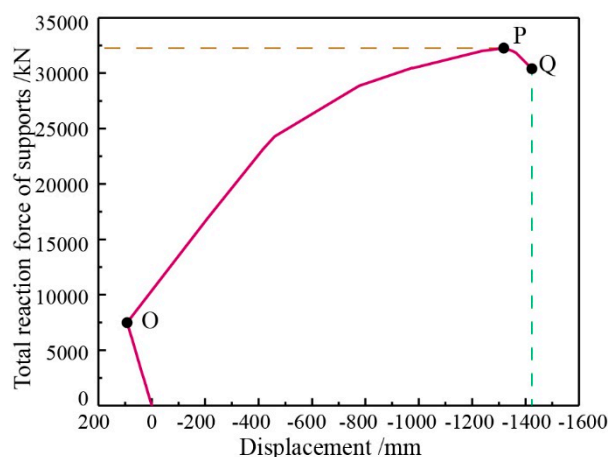


Figure 10. Force-displacement of the intact structure.

3.6. Remove Sensitive Areas Nodes

In order to comprehensively analyze the influence of node failures on the overall structure, several nodes in the sensitive areas in Figure 7 were removed, including 2, 3, 4, and 6 nodes, as shown in

Figure 11. Since the structure is a double-layer structure, to better understand the location of removed nodes, the upper chord layer and the lower chord layer were used to show the specific location of the removed nodes. For example, two nodes were removed in the grid area in Figure 11(1a), with the black solid dots in Figure 11(1b,c) that indicate the specific removed nodes.

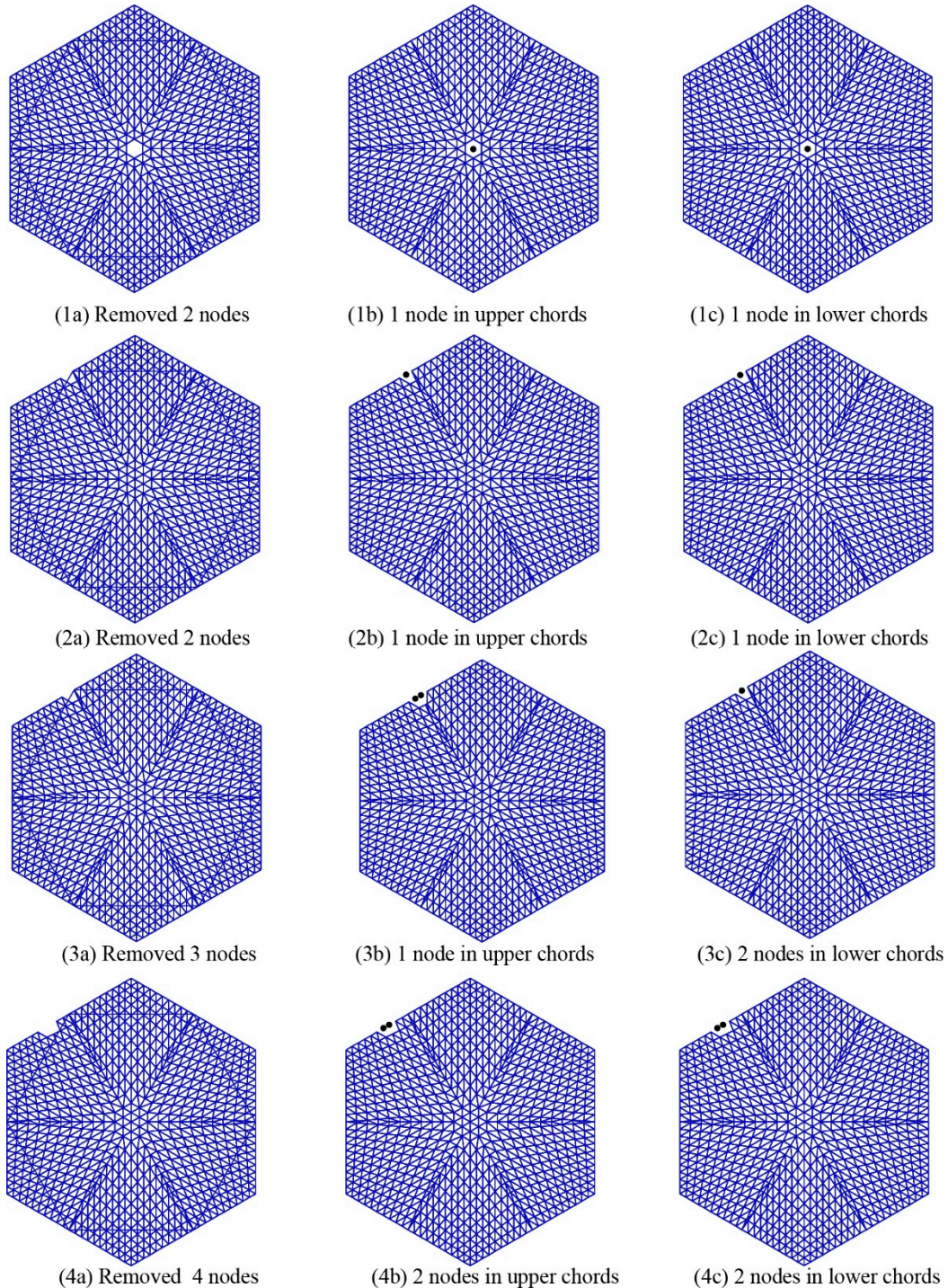


Figure 11. Cont.

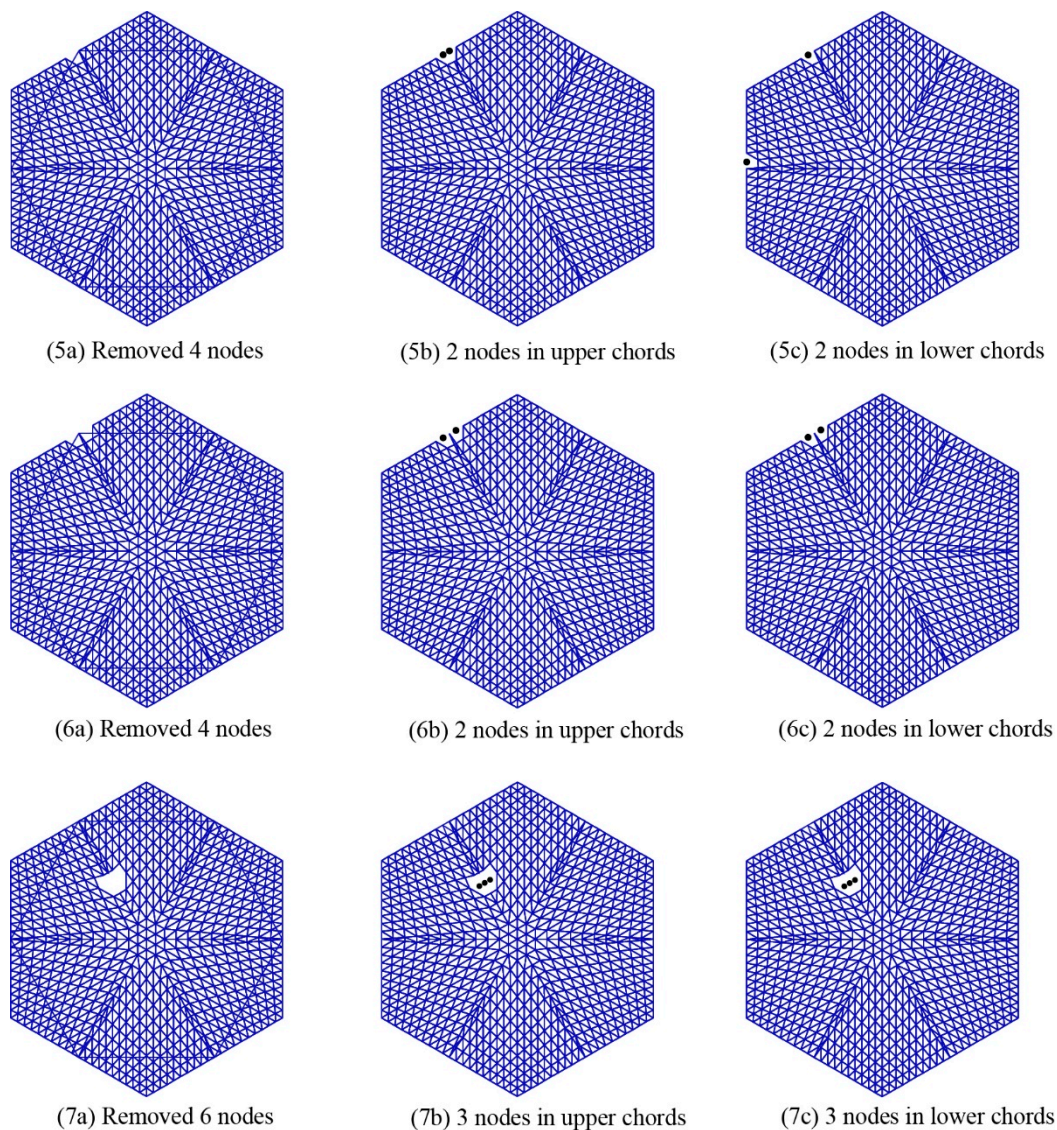


Figure 11. Location of removed nodes.

The nodes removed in Figure 11 include sensitive areas, such as the support area, the daylighting area, the flat grid area, and the fringe truss area. The equivalent load transient unloading method, based on dynamic time history analysis was used to analyze the residual structure after the removal of the nodes. The ratio between the stress of structural member and the yield stress of material is defined as the stress ratio. The upper limit of the stress ratio of the members was set to 1.0. In the software of SAP2000, the stress ratio of each member in the structure was calculated and displayed. If the stress ratio was greater than 1.0, the components fell into their plastic deformation stage. The dynamic damage index D of the structure was calculated according to formula (1), and the results are shown in Table 1.

According to the value of the dynamic damage index D , the damage levels of the structure with the different nodes removed can be classified as in Table 1. The latter shows that the structures of Figure 11(1a,2a,4a) and Figure 11(7a) are at a basic intact level I. The structure of Figure 11(3a) is at a medium damaged level III. The structure of Figure 11(5a) is at a severe damaged level III. The structure of Figure 11(6a) is at a progressively collapsed level V.

In the distribution of the structural plastic hinges, $B \rightarrow IO \rightarrow LS \rightarrow CP \rightarrow C \rightarrow D \rightarrow E$ indicates that the development degree is from low to high. Points B, C, D and E represent the yield, ultimate strength,

residual strength and failure of member, respectively. Points IO, LS and CP represent the capacity level of the plastic hinge, corresponding to Immediate Occupancy (IO), Life Safety (LS) and Performance Levels of Collapse Prevention (CP). These points are reflected in the structure by different colors. The structure of Figure 11(6a) was specifically analyzed and compared with the intact structure. The displacement–time curve of vertex A of the intact structure and the structure of Figure 11(6a) are shown in Figure 12. As the vibration continued, the difference between the vertex displacements of the two structures became larger and larger. At 5.28 s, the maximum displacement of 906 mm was reached, while the vertex displacement of the structure of Figure 11(6a) was −1111 mm, and the displacement of the intact structure was −205 mm. Figure 12 shows the failure process of the structure described in Figure 11(6a). The plastic hinges first appeared near the support of the removed nodes and then developed outward. The two supports adjacent to the removed nodes encountered serious damages because the load of the support of the removed nodes decreased, thus leading the reduced part to be dragged by the two adjacent supports. A large number of members whose stress ratios exceeded 1.0 can be observed. The number of upper chord layers was 790, the number of web member layers was 524, and the number of lower chord layers was 719. The cumulative plastic energy dissipation increased, leading to a final energy of 98,052,095 J. The maximum displacement of the structure was −10,482 mm. The dynamic damage index D was 9.459. The structure of Figure 11(6a) encountered a progressive collapse.

Table 1. Analysis results of the structure from which the nodes were removed.

Number of Removed Nodes	Position	Number of Members Whose Stress Ratio Exceeded 1.0			δ_m/mm	$\int dE/J$	D	Damage Level
		Upper Chord Layer	Web Member Layer	Lower Chord Layer				
2 nodes	Figure 11(1a)	0	0	1	−203	25,458	0.143	I
	Figure 11(2a)	21	32	64	−214	144,074	0.153	I
3 nodes	Figure 11(3a)	25	37	63	−716	5,566,350	0.624	III
4 nodes	Figure 11(4a)	18	23	39	−213	116,495	0.152	I
	Figure 11(5a)	149	50	147	−925	7,073,455	0.804	IV
	Figure 11(6a)	790	524	719	−10,482	98,052,095	9.459	V
6 nodes	Figure 11(7a)	2	2	0	−203	60,760	0.144	I

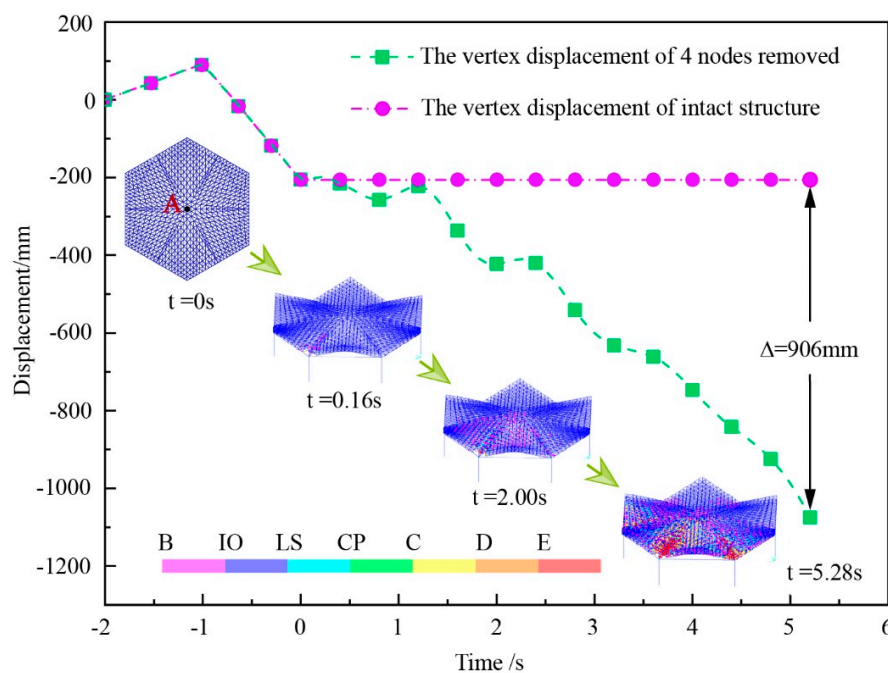


Figure 12. Displacement time curve of vertex A.

4. Construction and Design of the Sleeve Structure

The sleeve structure was composed of an inner core and a sleeve with a gap. The length of the sleeve was slightly smaller than that of the inner core, as shown in Figure 13a. When the inner core was under pressure, the sleeve mainly provided lateral restraint for the core and protected it from unexpected loads. High-order buckling modes can appear in the inner core to improve the load-bearing capacity of the member. Through the point contact or line contact between the core and the sleeve, the stress of the inner core under the restraint of the flexible sleeve reached the yield stress. The part of the inner core extending out of the sleeve was the weak part of the sleeve structure. This part was prone to buckling, thus determining the decline in the inner core bearing capacity. The structure of Figure 13a was adopted for the reinforcement of this part. The part of the core extending from the sleeve was reinforced with a circular stiffening ring that had a thickness not lower than the wall thickness of the inner core. The inner wall of the sleeve and the outer wall of the stiffening ring required a net of at least 2 mm gap. One end of the inner core and the sleeve was a sliding hinge support, as shown in Figure 13a,b; the other end of the core and the sleeve had a fixed hinge support, as shown in Figure 13a,c. With this configuration, the inner core bore all the external load, and the sleeve could only resist the bending of the inner core. The arrangement of the sleeve structure in the long-span space structure was connected by the hinge of the inner core and the structure. The size and relevant design parameters of the sleeves were calculated according to the literature [19,30], as shown in Table 2. The steel pipe number in the table indicates the members with sleeves that are required to be arranged in the structure—namely inner cores. The stress of these inner cores can reach the yield stress. The dimension specifications and lengths are listed in Table 2. The sleeve sizes are the specification of the round steel pipes added on the outside of these inner cores. The sleeve and the steel pipe in the original structure together constitute the sleeve structure.

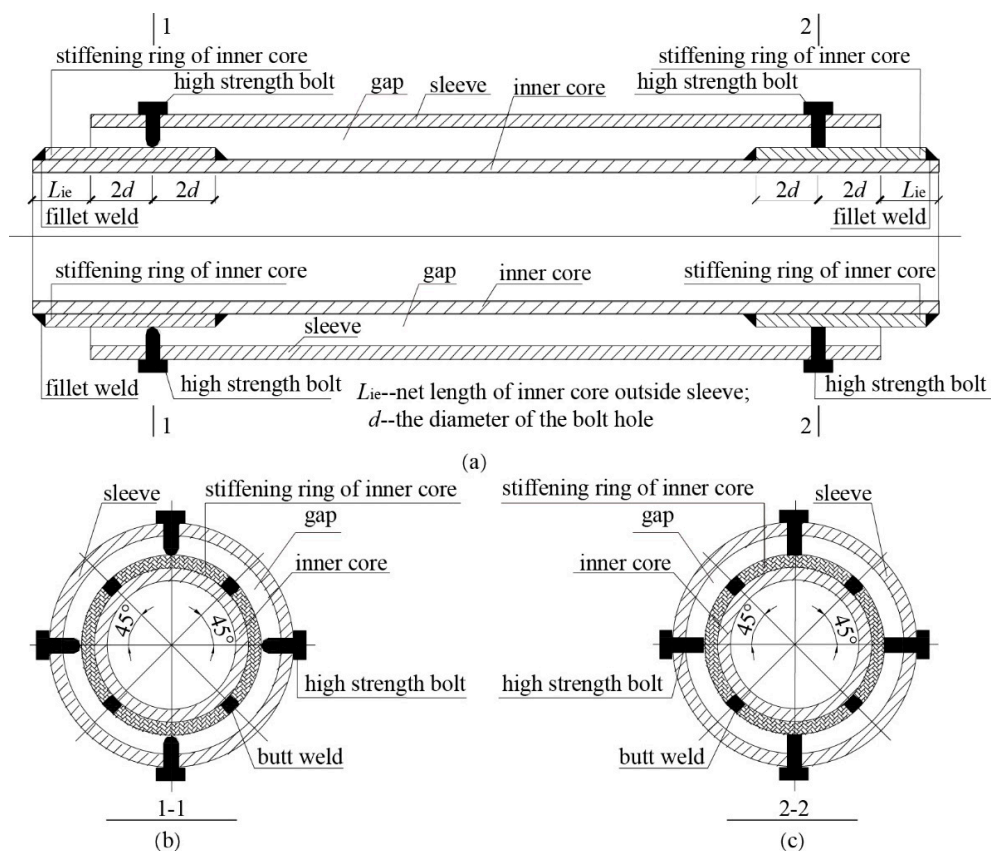


Figure 13. Connection details between the inner core and the sleeve: (a) Profile of sleeve structure; (b) Sliding hinge support; (c) Fixed hinge support.

Table 2. Basic configuration of the sleeve structure in the system.

Number of Steel Pipe	Size of Steel Pipe/mm × mm	Length of Steel Pipe/mm	Size of Sleeve/mm × mm	β	\bar{P}_{iy}/\bar{P}_E	$\bar{M}_{emax}/\bar{M}_{ep}$	Contact Mode between Sleeve and Inner Core
1	68 × 3.5	3801	102 × 6.0	0.225	4.224	0.751	line contact
2	89 × 3.5	2478	108 × 5.0	0.654	1.023	0.086	point contact
3	89 × 3.5	2478	108 × 5.0	0.654	1.023	0.086	point contact
4	68 × 3.5	3801	102 × 6.0	0.225	4.224	0.751	line contact
5	70 × 3.5	4130	114 × 4.0	0.194	4.692	0.946	line contact
6	219 × 6.0	5147	245 × 6.5	0.658	0.712	0.052	point contact
7	60 × 3.5	3059	89 × 3.5	0.289	3.562	0.978	line contact
8	89 × 3.5	3000	108 × 5.0	0.654	1.499	0.155	point contact
9	83 × 3.5	3283	95 × 3.5	0.656	2.075	0.33	line contact
10	219 × 6.0	5147	245 × 6.5	0.658	0.712	0.052	point contact
11	219 × 6.0	5147	245 × 6.5	0.658	0.712	0.052	point contact
12	219 × 6.0	5147	245 × 6.5	0.658	0.712	0.052	point contact
13	219 × 6.0	5147	245 × 6.5	0.658	0.712	0.052	point contact

Note: β denotes the ratio of the bending stiffness of the core to the sleeve; \bar{P}_{iy} denotes the yield load of the core; \bar{P}_E denotes the buckling critical load of the core; \bar{M}_{emax} denotes the maximum bending moment of the sleeve under load; \bar{M}_{ep} denotes the plastic hinge moment of the sleeve.

5. Control of Sleeve Structure to Progressive Collapse

5.1. Definition of Plastic Hinge

There are three types of hinge attributes in SAP2000 software: default hinge attribute; user specified hinge attribute; generated hinge attribute. Only default hinge properties and user specified hinge properties can be assigned to truss elements. SAP2000 provides default hinge properties in accordance with FEMA356 specification [31]. In this paper, the axial force hinge with deformation control (ductility) was selected.

5.2. Simulation of the Sleeve Structure

The sleeve structure was formed by arranging a sleeve outside the steel pipe in the structure, with the stress of the inner core that can reach its yield stress [19]. Wu et al. set the internal force of the compressed inner cores as the yield stress to simulate the sleeve structures, and applying them to the grid structure can improve the ultimate bearing capacity of the structure [32]. For the steel pipe that needed to be sleeved, the yield stress of the plastic hinge was set to 345 N/mm² in SAP2000 to simulate the sleeve structure.

5.3. Arrangement of the Sleeve Structure

The progressive collapse occurred in the structure described in Figure 11(6a). In this structure, three different methods were used for arranging the sleeve structures for the compression steel pipes. They were: (1) arranging sleeve structures on the members where the plastic hinge first appears; (2) arranging sleeve structures on the members with the largest displacement; (3) arranging sleeve structures on the members with the maximum force.

At the initial stage of the collapse, five plastic hinge members first appeared and were numbered 1, 2, 3, 4 and 5, as shown in Figure 14a. In the process of collapse, the point with the largest displacement appeared at point a. The vertical members connected with point a were numbered 6, 7, 8 and 9, as shown in Figure 14b. There were two members with the greatest force in the process of collapse and they were numbered 10 and 11, as shown in Figure 14c.

5.3.1. One Sleeve Was Arranged at Different Positions

(1) At the position of the plastic hinge: arranged sleeve for member No. 5; (2) At the position with the largest displacement: arranged sleeve for member No. 9; (3) At the position of maximum force:

arranged sleeve for member No. 11. The results of the comparative analysis of the above three models are shown in Table 3.

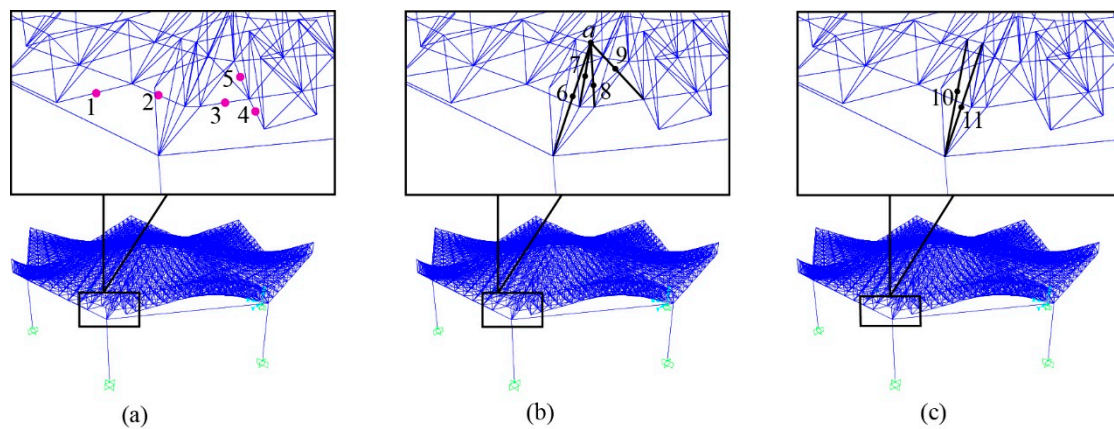


Figure 14. Position of sleeve structures: (a) position where the plastic hinge appears first; (b) position with the largest displacement; (c) position of maximum force.

Table 3. Analysis results of the structure with one sleeve structure.

Number of Member Arranged Sleeved	Number of Members Whose Stress Ratio Exceeded 1.0			δ_m/mm	$\int dE/J$	D	Damage Level
	Upper Chord Layer	Web Member Layer	Lower Chord Layer				
5	792	528	714	-10,650	97,895,621	9.610	V
9	769	516	707	-10,244	96,058,972	9.285	V
11	808	536	720	-10,483	100,025,894	9.539	V

As can be seen from Table 3, a sleeve is arranged in three different positions of the structure, and there is a large number of members whose stress ratios exceed the limit. As the dynamic damage index D of these three models is large, the arrangement of one sleeve cannot control the progressive collapse of the structure.

5.3.2. Two Sleeves Were Arranged at Different Positions

(1) At the position of the plastic hinges: arranged sleeves for members No. 4 and 5; (2) At the position with the largest displacement: arranged sleeves for members No. 6 and 9; (3) At the position of maximum force: arranged sleeve for members No. 10 and 11. The results of the comparative analysis of the above three models are shown in Table 4.

Table 4. Analysis results of the structure with two sleeve structures.

Number of Member Arranged Sleeved	Number of Members Whose Stress Ratio Exceeded 1.0			δ_m/mm	$\int dE/J$	D	Damage Level
	Upper Chord Layer	Web Member Layer	Lower Chord Layer				
4,5	787	521	709	-10,435	96,982,357	9.439	V
6,9	771	522	710	-10,444	97,253,274	9.451	V
10,11	36	15	36	-226	110,444	0.161	I

As described in Table 4, by comparing the three different positions of the structure, it was found that the final displacement of node a , on which the maximum displacement was located, was -69 mm when the sleeves were arranged on the 10 and the 11 members. The number of members with over-limit stress ratio in the upper chord layer decreased from 790 to 36, the number of web member layer decreased from 524 to 15, and the number of lower chord layers decreased from 719 to 36.

The maximum displacement of the structure was -226 mm, located at vertex a , as shown in Figure 15a. The cumulative plastic energy dissipation was reduced from 98,052,095 J to 110,444 J, while the dynamic damage index D decreased from 9.459 to 0.161. According to the dynamic damage index, it can be seen that the structure is basically intact after damage, with the damage being at level I. However, when two sleeves were arranged at the other two positions, the displacement of the node a became very large, as shown in Figure 15b. The dynamic damage index D values were 9.439 and 9.451, respectively, with the damage being at level V.

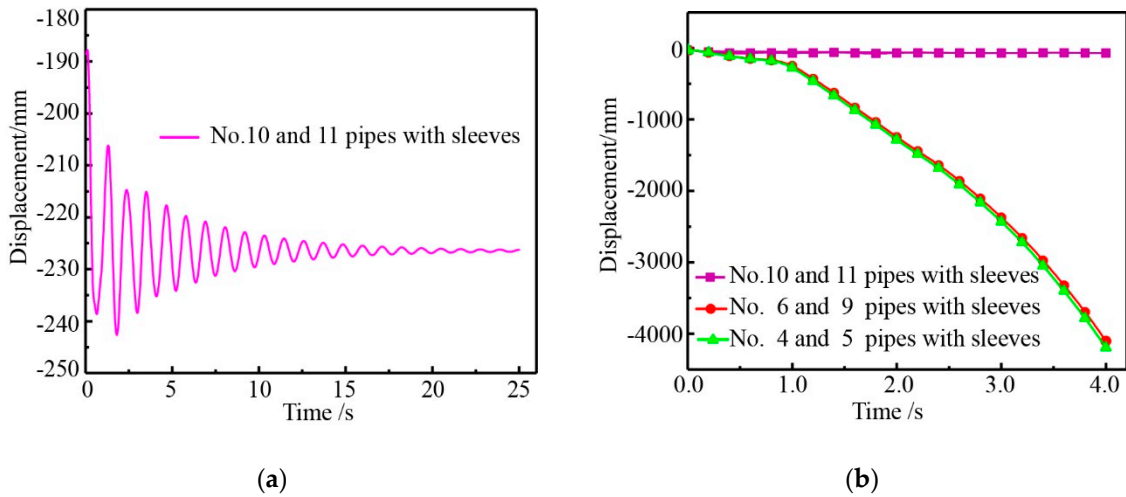


Figure 15. The displacement–time curve of nodes A and a : (a) node A; (b) node a .

The responses of the structure with no sleeves and those with sleeves in members 10 and 11 are compared in Figure 16. The results show that the maximum displacement decreased from $-10,482$ mm to -69 mm when the two sleeves were placed in the position with the maximum force. The development of the final plastic hinges were near the removed nodes, with their range being very limited. The progressive collapse of the structure was effectively controlled.

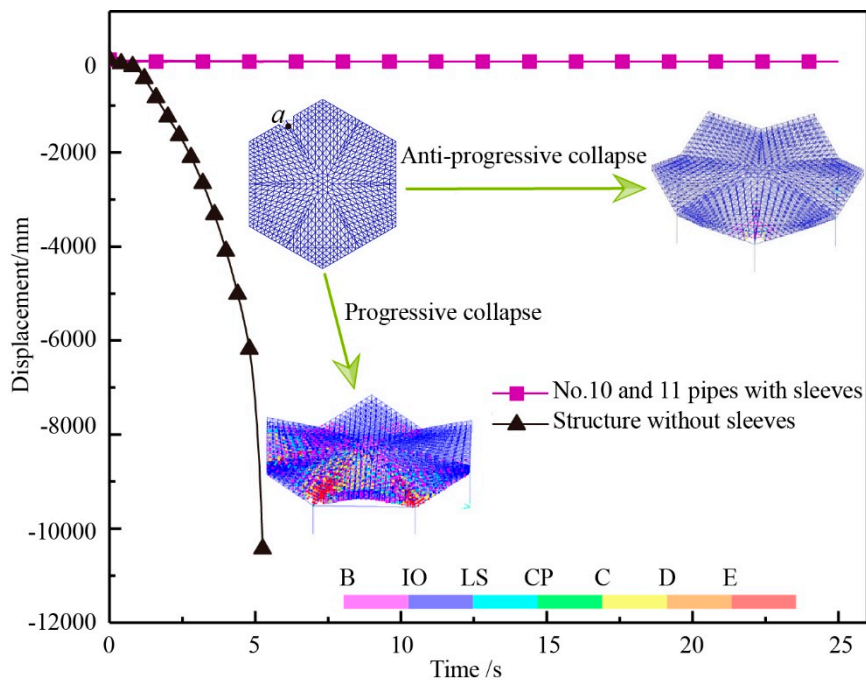


Figure 16. The displacement–time curve of node a .

5.3.3. Principle of Sleeve Structure Arrangement

It can be seen from the previous analysis that, in a structure experiencing a progressive collapse, the sleeves were arranged at the position where the plastic hinges appeared first and at the position with the largest displacement, which had a poor control effect on the structural deformation. When the sleeves were arranged at the position with the maximum force, the structural deformation could be controlled more effectively. In order to control the progressive collapse failure of the long-span prestressed double-layer composite torsional latticed shell, the sleeves should be arranged on the members with the maximum force.

6. Control of Sleeve Structure to Medium Damage

The model described in this section is the structure of Figure 11(5a), with medium damage. According to the above sleeve structure arrangement principles, the sleeves should be arranged at the position with the maximum force in the structure. In the structure of Figure 11(5a), the sleeves are arranged for members 12 and 13 with the maximum force, as shown in Figure 17.

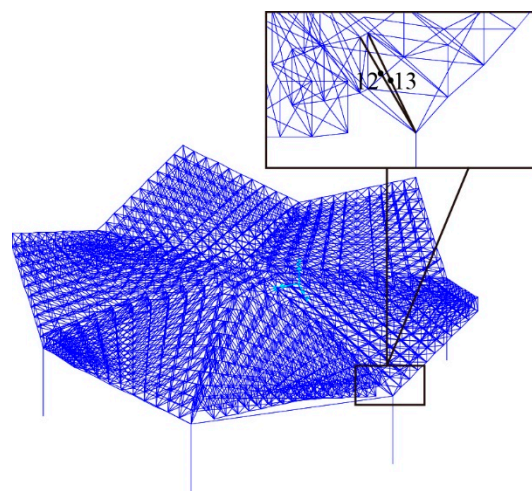


Figure 17. Position of the sleeve structures.

It can be seen from Table 5 that the number of members with over-limit stress ratio in the upper chord layer decreased from 149 to 31, the web member layer decreased from 50 to 22, the lower chord layers decreased from 147 to 56, the maximum displacement from -925 mm to -244 mm, and the cumulative plastic energy consumption from $7,073,455$ J to $357,216$ J. The dynamic damage index of the structure was reduced from 0.804 to 0.179 . According to the dynamic damage index D , it can be deduced that the structure was basically intact after damage, with the damage being at level I.

Table 5. Analysis results of the structure with two sleeve structures.

Number of Members Arranged Sleeves	Number of Members Whose Stress Ratio Exceeded 1.0			δ_m/mm	$\int dE/J$	D	Damage Level
	Upper Chord Layer	Web Member Layer	Lower Chord Layer				
12,13	31	22	56	-244	$357,216$	0.179	I

In Figure 18, the displacement of vertex A was -244 mm, and after that the sleeves were arranged on the members 12 and 13. Through the comparison between the sleeve arrangement in the structure of Figure 11(5) and that without sleeves arrangement, it can be seen that, after the sleeves were arranged, the range of plastic hinges was relatively small. This mainly occurs near the removed nodes, with the

structure being slightly damaged. Contrarily, for the structure without sleeves, the plastic hinges appeared in a larger range, with the structure being in a basically intact after damage state.

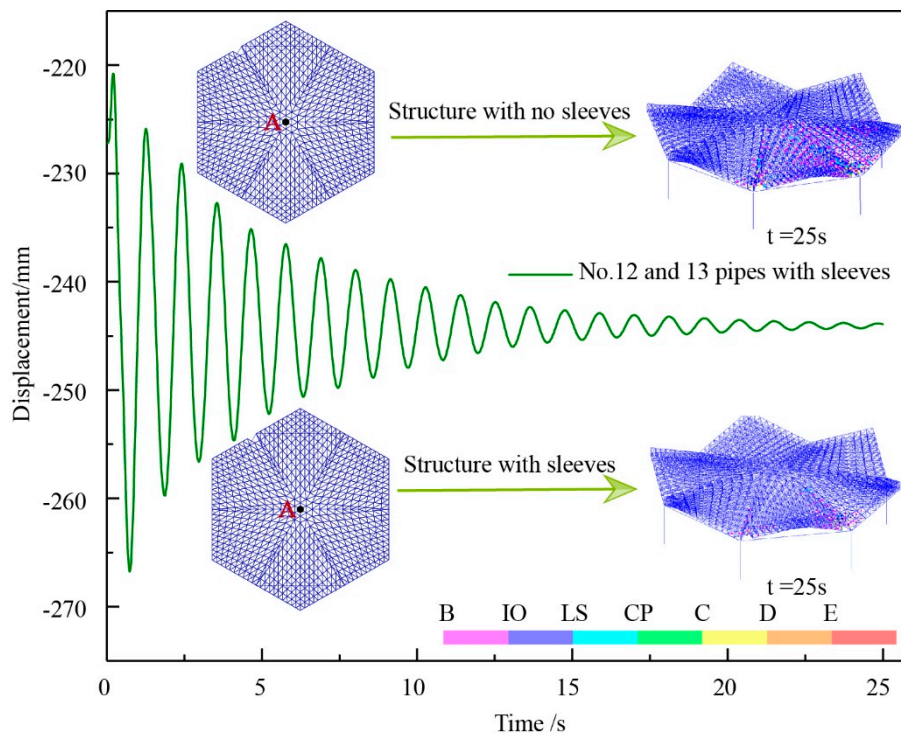


Figure 18. The displacement-time curve of node A.

From the above analysis, it can be seen that the sleeves were arranged in the members with the maximum force, thus reducing the damage of the structure from a severe damage level to a basic intact damage level.

7. Conclusions

In this paper, a new dynamic damage evaluation index considering the maximum displacement and plastic cumulative energy dissipation is proposed for a long-span prestressed double-layer composite torsional reticulated shell structure. The damage assessment of the structure was analyzed by removing the nodes in sensitive areas. The control effect of three different sleeve structures arrangement on structural failure was studied. The conclusions are as follows:

- (1) The new dynamic damage index can quickly and efficiently evaluate the structural damage.
- (2) When the four nodes near the support were removed, the structure encountered a progressive collapse failure.
- (3) The results show that the sleeves are arranged at the position where the plastic hinges appear first and the displacement is the largest, which has a poor control effect on the structural damage; when two sleeves are arranged at the maximum force position, the structure with progressive collapse and severe damage is controlled, with the damage grade of the structure being in a basically intact after damage state.

The results are based on reasonable finite element models, which were prepared for the later experiments. The analysis results will be verified by experiments in the future.

Author Contributions: Conceptualization, X.Z. and Y.H.; methodology, H.L.; formal analysis, B.S.; investigation, J.Z.; writing—original draft preparation, X.Z. All authors have read and agreed to the published version of the manuscript.

Funding: This work was fully supported by the National Natural Science Foundation of China under contract No. 51468007.

Conflicts of Interest: The authors declare no conflict of interest.

References

1. Martin, R.; Delatte, N.J. Another look at Hartford civic center coliseum collapse. *J. Perform. Constr. Fac.* **2001**, *15*, 31–36. [[CrossRef](#)]
2. Hansson, M.; Larsen, H.J. Recent failures in glulam structures and their causes. *Eng. Fail. Anal.* **2005**, *12*, 808–818. [[CrossRef](#)]
3. Jorgen, M.-A.; Philipp, D. Robustness of large-span timber roof structures—Two examples. *Eng. Struct.* **2011**, *33*, 3113–3117.
4. Zhao, X.; Yan, S.; Chen, Y. Comparison of progressive collapse resistance of single-layer latticed domes under different loadings. *J. Constr. Steel Res.* **2017**, *129*, 204–214. [[CrossRef](#)]
5. Lu, X.; Lin, K.; Li, C.; Li, Y. New analytical calculation models for compressive arch action in reinforced concrete structures. *Eng. Struct.* **2018**, *168*, 721–735. [[CrossRef](#)]
6. Ventura, A.; De Biagi, V.; Chiaia, B. Structural robustness of RC frame buildings under threat-independent damage scenarios. *Struct. Eng. Mech.* **2018**, *65*, 689–698.
7. Gernay, T.; Gamba, A. Progressive collapse triggered by fire induced column loss: Detrimental effect of thermal forces. *Eng. Struct.* **2018**, *172*, 483–496. [[CrossRef](#)]
8. Adam, J.M.; Parisi, F.; Sagaseta, J.; Lu, X. Research and practice on progressive collapse and robustness of building structures in the 21st century. *Eng. Struct.* **2018**, *173*, 122–149. [[CrossRef](#)]
9. GSA. *Progressive Collapse Analysis and Design Guidelines for New Federal Office Buildings and Major Modernization Projects*; US General Services Administration: Washington, DC, USA, 2003.
10. DOD UFC 4-023-03. *Design of Buildings to Resist Progressive Collapse*; US Department of Defense: Washington, DC, USA, 2009.
11. CECS 392-2014. *Code for Anti-Collapse Design of Building Structures*; China Association for Engineering Construction Standardization: Beijing, China, 2015.
12. JSSC & CTBUH. *Guidelines for Collapse Control Design—Construction of Steel Buildings with High Redundancy*; Japan Iron and Steel Federation: Tokyo, Japan, 2005; Volume 1.
13. Xu, Y.; Han, Q.H.; Parke, G.A.R.; Liu, Y.M. Experimental study and numerical simulation of the progressive collapse resistance of single-layer latticed domes. *J. Struct. Eng.* **2017**, *143*, 1–15. [[CrossRef](#)]
14. Zhu, N.H.; Ye, J.H. Structural vulnerability of a single-layer dome based on its form. *J. Eng. Mech.* **2014**, *140*, 112–127.
15. Sheidaii, M.R.; Parke, G.A.R.; Abedi, K.; Behraves, A. Dynamic Snap-Through Buckling Of Truss-Type Structures. *Int. J. Space Struct.* **2001**, *16*, 85–94. [[CrossRef](#)]
16. Zhou, H.T.; Zhang, Y.G.; Feng, F.; Wu, J.Z. Progressive collapse analysis of reticulated shell structure under severe earthquake loading considering the damage accumulation effect. *J. Perform. Constr. Fac.* **2018**, *32*, 1–10. [[CrossRef](#)]
17. Li, S.; Wang, D.S. Progressive collapse resistance design of long-span steel structures. *J. Sichuan Univ.* **2011**, *43*, 20–28. (In Chinese)
18. Zhu, Y.; Feng, J.; Cai, J.; Zhang, L. Analysis on progressive collapse resistance of truss string structure of Meijiang Exhibition Center. *J. Build. Struct.* **2013**, *34*, 45–53. (In Chinese)
19. Hu, L.; Shen, B.; Ma, K.J.; Deng, C.G.; Yan, B.W. A mechanical model and experimental investigations for axially compressed sleeved column. *J. Constr. Steel Res.* **2013**, *89*, 107–120. [[CrossRef](#)]
20. Hu, B.; Gao, B.; Zhan, S.; Zhang, C. Theoretical and experimental study on load-carrying capacity of combined members consisted of inner and sleeved tubes. *Struct. Eng. Mech.* **2013**, *45*, 129–144. [[CrossRef](#)]
21. Shen, J.; Seker, O.; Sutchiewcharn, N. Cyclic behavior of buckling-controlled braces. *J. Constr. Steel Res.* **2016**, *121*, 110–125. [[CrossRef](#)]
22. Zhang, C.; Deng, C. Theoretical study of sleeved compression members considering the core protrusion. *Struct. Eng. Mech.* **2018**, *66*, 783–792.
23. Zhang, C.; Deng, C. Static behaviors of buckling-monitoring members. *Eng. Struct.* **2019**, *178*, 55–69. [[CrossRef](#)]

24. Sadamoto, S.; Tanaka, S.; Taniguchi, K.; Ozdemir, M.; Bui, T.Q.; Murakami, C.; Yanagihara, D. Buckling analysis of stiffened plate structures by an improved meshfree flat shell formulation. *Thin Walled Struct.* **2018**, *117*, 303–313. [[CrossRef](#)]
25. Sadamoto, S.; Ozdemir, M.; Tanaka, S.; Taniguchi, K.; Yu, T.T.; Bui, T.Q. An effective meshfree reproducing kernel method for buckling analysis of cylindrical shells with and without cutouts. *Comput. Mech.* **2017**, *59*, 919–932. [[CrossRef](#)]
26. Park, Y.J.; Ang, A.H.S. Mechanistic seismic damage model for reinforced concrete. *J. Struct. Eng.* **1985**, *111*, 722–739. [[CrossRef](#)]
27. Fu, F.; Parke, G.A.R. Assessment of the Progressive Collapse Resistance of Double-Layer Grid Space Structures Using Implicit and Explicit Methods. *Int. J. Steel Struct.* **2018**, *18*, 1–12. [[CrossRef](#)]
28. Nie, G.; Liu, K.; Zhi, X. Performance-based seismic design of reticulated shells. *Chin. Civil Eng. J.* **2018**, *51*, 13–17. (In Chinese)
29. Zhang, M.; Zhang, K.; Li, Q.; Zhou, G. Parametric analysis of seismic performance of single-layer reticulated shell structure based on strain energy density. *Chin. Civil Eng. J.* **2016**, *49*, 11–18. (In Chinese)
30. Shen, B.; Ma, K.J.; Hu, L.; Deng, C.G. Theoretical and Experimental Analysis of Axial Compression Sleeved Column and Its Design. *J. Hunan Univ. (Nat. Sci. Ed.)* **2013**, *40*, 33–39. (In Chinese)
31. FEMA356. *Prestandard and Commentary for the Seismic Rehabilitation of Buildings*; Federal Emergency Management Agency: Washington, DC, USA, 2000.
32. Wu, T.; Deng, C.; Shen, B. Buckling control and application of axial compression steel member. *J. Southeast Univ. (Nat. Sci. Ed.)* **2009**, *39*, 53–57. (In Chinese)



© 2020 by the authors. Licensee MDPI, Basel, Switzerland. This article is an open access article distributed under the terms and conditions of the Creative Commons Attribution (CC BY) license (<http://creativecommons.org/licenses/by/4.0/>).